

Absolute parameters of the three totally-eclipsing W UMa stars NSVS 2443858, NSVS 780649 and V1098 Her

Velimir Popov¹, Francesco Acerbi² and Carlo Barani³

¹ Department of Physics and Astronomy, Shumen University, 115 Universitetska str., 9700 Shumen, Bulgaria

² Via Zoncada 51, 26845 Codogno (LO), Italy; acerbifr@tin.it

³ Via Molinetto 35, 26845 Triulza di Codogno (LO), Italy

Received 2020 November 21; accepted 2021 April 30

Abstract We present the first photometric analysis of three totally-eclipsing W UMa binaries, NSVS 2443858, NSVS 780649 and V1098 Her. The absolute astrophysical parameters of the stellar components were determined by means of Gaia distances and light curve solutions. The results show that: (i) Two of the systems, NSVS 2443858 and V1098 Her, are of A subtype while the obtained temperature of the secondary component of NSVS 780649 indicates that it is a W-subtype system; (ii) The estimated mass ratios approach the lower limit of the mass ratio assumed by researchers in recent years so our targets could be classified as extreme mass ratio binary (EMRB) systems; (iii) All the systems have deep contact configurations, so they also are deep low mass ratio (DLMR) systems; (iv) The components of our systems are stars of F and G spectral type and undergo total eclipses; (v) The sum $0.871 M_{\odot}$ of the component masses of NSVS 780649 is below the mass limit of 1.0-1.2 M_{\odot} assumed for the known contact binary stars.

Key words: techniques: photometric — binaries: eclipsing — stars: fundamental parameters — stars: individual

1 INTRODUCTION

Most W UMa-type stars are binary systems with periods shorter than a day whose light curves reveal continuous changes of brightness and have equal (or nearly equal) primary and secondary eclipse depths (Jayasinghe et al. 2020). These observational characteristics are explained by configuration of two late type stars in contact with each other, that share a common convective envelope lying between the inner and outer critical Roche surfaces. A large-scale energy transfer between the components results in almost equalizing surface temperatures over the entire system despite very different masses. The binary components acquire almost identical surface brightness (Lucy 1968b,a).

Contact binaries can be divided into two groups: A-subtype and W-subtype (Binnendijk 1970). Those with a primary minimum being a transit of the less massive component are called A-type, and when it is an occultation the binary is of W-type.

Of particular interest are the W UMa stars with wide total eclipses (in phase units), which turn out to have a low mass ratio. This group includes the so-called

deep, low-mass ratio contact binary (DLMCB) stars that have mass ratios q less than 0.25 and fill-out factor f greater than 50% (Qian et al. 2006). These systems provide a key for understanding the late evolution of binaries and the formation of blue stragglers and FK Com-type stars (Eggleton & Kiseleva-Eggleton 2001). After the pioneering work of Webbink (1976) about the existence of a cut-off in mass ratio q_{\min} (for $q < q_{\min}$ the binary system quickly merges into a single, rapidly rotating star), several investigations appeared on determination of the low mass ratio limit: $q_{\min} \sim 0.09$ (Rasio & Shapiro 1995); $q_{\min} \sim 0.071-0.076$ (Li & Zhang 2006); $q_{\min} \sim 0.094-0.109$ (Arbutina 2007); $q_{\min} \sim 0.070-0.074$ (Arbutina 2012); $q_{\min} \sim 0.044$ (Yang & Qian 2015).

The theoretical investigations were prompted by the discoveries of binaries with extremely low mass ratios, as for example, those in table 3 in Kjurkchieva et al. (2018).

Using the distances available in the Gaia database (Bailer-Jones et al. 2018), the absolute parameters of a large number of eclipsing binary stars can be determined with acceptable accuracy. Measuring the absolute parameters of close binary stars are milestones in investigating

Table 1 Parameters of the Targets from the VSX Database

Target	RA	Dec	Period (d)	Mag.	Ampl.	Ref.
NSVS 2443858	08:37:56.64	+55:48:23.0	0.298207	10.93	0.28	(Gettel et al. 2006)
NSVS 780649	09:06:42.36	+70:03:24.6	0.28119313	13.55	0.92	(Woźniak et al. 2004)
V1098 Her	17:39:37.21	+50:12:02.6	0.352268564	12.44	0.38	(Akerlof et al. 2000)

Notes: The coordinates of NSVS 780649 (GSC 04379-01487) from the VSX database are wrong. The correct coordinates are those of GSC 04379–01487, RA 09:06:43.34, Dec +70:03:29.23.

Table 2 Log of Photometric Observations

Target	UT Date (yyyymmdd)	Exposures (g' , i') (s)	Number (g' , i')	Mean error (g' , i') (mag)
NSVS 2443858	2020 Jan 22	60, 120	124, 124	0.005, 0.006
	2020 Jan 23	60, 120	95, 95	0.005, 0.005
NSVS 780649	2020 Feb 16	120, 120	59, 59	0.009, 0.016
	2020 Feb 17	120, 120	137, 137	0.007, 0.013
V1098 Her	2020 Aug 9	60, 120	115, 115	0.007, 0.008
	2020 Aug 10	60, 120	68, 68	0.005, 0.006
	2020 Aug 13	60, 120	115, 115	0.009, 0.010

the processes of energy transfer, mass exchange, mass loss and the evolutionary status and final fate (tight binaries or merger). Contact binary stars are suitable for studying the described processes, as these stars leave the main sequence (MS), sometimes have small mass ratios, their periods are variable on different time scales, show various stellar activity, and are also widespread and are easily detectable. The population of overcontact W UMa type binaries in the solar neighborhood is about 95% from all eclipsing binary variable stars (Berdyugina 2005). Our results also contribute to the enrichment of statistical data on W UMa stars with known absolute parameters.

Precise determinations of the mass ratios of eclipsing binaries are necessary conditions for estimating the values of the component stellar radii, masses and luminosities. Due to the impossibility of obtaining qualitative spectral data for low-brightness eclipsing binary stars and thus determining their mass ratios q , the way to do this with confidence is to rely on light curve solutions for W UMa systems with high inclinations that show total eclipses (Rucinski 2001; Terrell & Wilson 2005). To constrain the values of the mass ratios derived from the light curve solutions of our targets, we applied a q -search method. This method ensures great reliability for the estimated values of the stellar parameters.

This paper presents photometry of three W UMa systems (NSVS 2443858, NSVS 780649 and V1098 Her). Their light curves contain flat sections in the minima which mean that the binary components perform total eclipses.

2 OBSERVATIONS AND DATA REDUCTION

Table 1 presents the available information about the targets from the American Association of Variable Star Observers (AAVSO) Variable Star Index (VSX) database.

The photometric observations of the targets were carried out with Sloan type filters in g' , i' bands. We employed the 30-cm Ritchey-Chrétien Astrograph located in the *IRIDA South* dome of the National Astronomical Observatory (NAO) Rozhen, Bulgaria. The astrograph works at $f/5$ (with focal reducer) and is equipped with an ATIK 4000M CCD camera (2048×2048 pixels, $7.4 \mu\text{m pixel}^{-1}$ and pixel-scale of $1.04 \text{ pixel arcsec}^{-1}$). Local seeing varied between 1.1 to 2.0 arcsec. We applied a photometric aperture of 4 pixels (4.8 arcsec) not using a special point spread function (PSF) technique. The field of view of the optical system is 35×35 arcmin. The log of our CCD photometric observations is presented in Table 2. Photometric data reduction was applied in the standard sequence (de-biasing, dark frame subtraction and flat-fielding) by the software AIP4WIN2.0 (Berry and Burnell 2006). Ensemble photometry was carried out with the automatic photometry tool LESVEPHOTOMETRY¹ (de Ponthire 2010). The mode for color transformation was applied along with the previously estimated transformation coefficients. To choose comparison and check stars for the ensemble photometry and to get photometric data for their magnitudes in the respective bands (Table 3), the catalog AAVSO Photometric All Sky Survey (APASS) Data Release 9 (DR9) catalog was referenced (Henden et al. 2015).

¹ www.dppobservatory.net

Table 3 Magnitudes of the Comparison and Check Stars

Label	Star ID	RA	Dec	g'	i'
Target	NSVS 2443858	08:37:56.64	+55:48:23.00	11.192	10.515
Chk	UCAC4 730–047606	08:37:23.73	+55:50:37.48	12.672	11.930
C1	UCAC4 731–047582	08:38:16.58	+56:00:37.95	11.919	10.958
C2	UCAC4 730–047639	08:38:45.75	+55:54:27.58	12.711	12.065
C3	UCAC4 730–047637	08:38:24.18	+55:50:48.50	12.022	11.424
C4	UCAC4 729–046330	08:38:11.71	+55:46:11.21	12.463	11.870
C5	UCAC4 729–046313	08:37:31.11	+55:44:22.42	12.156	11.216
C6	UCAC4 729–046316	08:37:47.02	+55:42:18.76	12.602	11.063
C7	UCAC4 729–046307	08:37:13.63	+55:39:39.04	12.206	11.576
Target	NSVS 780649	09:06:43.34	+70:03:29.23	13.560	12.861
Chk	UCAC4 801–019163	09:06:31.95	+70:05:27.32	13.405	12.967
C1	UCAC4 801–019185	09:07:43.67	+70:09:49.42	13.320	12.909
C2	UCAC4 801–019164	09:06:32.82	+70:10:21.83	13.252	12.716
C3	UCAC4 801–019147	09:05:18.16	+70:10:20.36	12.912	12.491
C4	UCAC4 800–019280	09:08:25.39	+69:58:29.84	13.003	12.578
C5	UCAC4 800–019257	09:06:34.81	+69:57:41.68	13.005	12.684
C6	UCAC4 801–019142	09:05:08.86	+70:06:53.40	13.185	12.353
C7	UCAC4 801–019156	09:05:48.68	+70:07:30.91	13.813	13.237
Target	V1098 Her	17:39:37.21	+50:12:02.60	12.500	11.968
Chk	UCAC4 702–057873	17:38:53.17	+50:13:33.98	13.474	12.512
C1	UCAC4 702–057920	17:40:07.18	+50:20:57.09	12.281	11.621
C2	UCAC4 702–057903	17:39:32.15	+50:17:10.25	12.979	12.267
C3	UCAC4 702–057858	17:38:35.01	+50:16:47.08	12.878	12.289
C4	UCAC4 701–060055	17:40:45.22	+50:04:26.11	12.390	11.756
C5	UCAC4 701–060029	17:39:54.95	+50:08:32.18	12.526	12.100
C6	UCAC4 701–060023	17:39:48.49	+50:08:27.77	11.938	11.294
C7	UCAC4 701–060000	17:39:17.28	+50:05:57.92	12.769	12.363
C8	UCAC4 701–059971	17:38:34.11	+50:07:00.82	12.024	11.379

Table 4 ToM for NSVS 2443858

Epoch (HJD)	Cycles	$O - C(1)$	$O - C(2)$	Reference
2451343.7602	−25242.0	−0.0294	−0.0008	NSVS (Woźniak et al. 2004)
2451343.9110	−25241.5	−0.0278	0.0008	NSVS (Woźniak et al. 2004)
2457412.6839	−4891.0	−0.0161	−0.0002	ASAS-SN (Shappee et al. 2014; Kochanek et al. 2017)
2457412.8334	−4890.5	−0.0157	0.0002	ASAS-SN (Shappee et al. 2014; Kochanek et al. 2017)
2458871.2542	0.0	−0.0002	−0.0005	This paper
2458871.4049	0.5	0.0014	0.0011	This paper
2458872.4470	4.0	−0.0002	−0.0006	This paper
2458872.5967	4.5	0.0004	0.0000	This paper

3 ORBITAL PERIOD VARIATIONS STUDY

With our observations, and times of minima (ToM) acquired from All-Sky Automated Survey for SuperNovae (ASAS-SN) (Shappee et al. 2014; Kochanek et al. 2017), Northern Sky Variability Survey (NSVS) (Woźniak et al. 2004) and literature, we were able to refine the ephemerides of the systems as shown below.

3.1 NSVS 2443858

NSVS 2443858 (GSC 03801–00264). From our observations we obtained the following ephemeris:

$$HJD(MinI) = 2458871.2544 + 0.2982119 \times E. \quad (1)$$

Using the ToM of Table 4, the ephemeris has been updated (Eq. (2)); a two degree polynomial ephemeris best fits available data.

$$HJD(Min I) = 2458871.2547(4) + 0.2982172(2) \times E + 3.970^{-10}(\pm 6.694^{-12}) \times E^2. \quad (2)$$

3.2 NSVS 780649

With the ToM of Table 5, the updated ephemeris is (Eq. (3))

$$HJD(Min I) = 2458897.4823(6) + 0.2811996(2) \times E. \quad (3)$$

Table 5 ToM for NSVS 780649

Epoch (HJD)	Cycles	$O - C(3)$	Reference
2457393.3472	-5349.0	0.0014	ASAS-SN (Shappee et al. 2014; Kochanek et al. 2017)
2457393.7661	-5347.5	-0.0014	ASAS-SN (Shappee et al. 2014; Kochanek et al. 2017)
2458896.4979	-3.5	-0.0002	This paper
2458897.3409	-0.5	-0.0008	This paper
2458897.4829	0.0	0.0006	This paper
2458897.6233	0.5	0.0004	This paper

Table 6 ToM for V1098 Her

Epoch (HJD)	Cycles	$O - C(4)$	$O - C(5)$	Reference
2451389.7388	-21809.0	-0.0012	0.0022	NSVS (Woźniak et al. 2004)
2451389.9109	-21808.5	-0.0053	-0.0018	NSVS (Woźniak et al. 2004)
2455417.3951	-10375.5	-0.0075	0.0003	(Arena et al. 2011)
2455417.3952	-10375.5	-0.0075	0.0003	(Brat et al. 2011)
2455417.3952	-10375.5	-0.0075	0.0003	(Brat et al. 2011)
2455454.3812	-10270.5	-0.0096	-0.0019	(Brat et al. 2011)
2455454.3815	-10270.5	-0.0093	-0.0016	(Arena et al. 2011)
2455641.6130	-9739.0	-0.0086	-0.0010	(Arena et al. 2011)
2455644.6084	-9730.5	-0.0074	0.0001	(Arena et al. 2011)
2455645.4866	-9728.0	-0.0099	-0.0023	(Arena et al. 2011)
2455654.4718	-9702.5	-0.0075	0.0000	(Hořková et al. 2013)
2455654.4722	-9702.5	-0.0072	0.0004	(Arena et al. 2011)
2455654.6468	-9702.0	-0.0087	-0.0011	(Arena et al. 2011)
2455654.6482	-9702.0	-0.0073	0.0003	(Hořková et al. 2013)
2455662.3975	-9680.0	-0.0079	-0.0003	(Hubscher et al. 2012)
2455662.5752	-9679.5	-0.0063	0.0012	(Hubscher et al. 2012)
2455669.4424	-9660.0	-0.0084	-0.0008	(Arena et al. 2011)
2455672.4381	-9651.5	-0.0070	0.0006	(Hubscher et al. 2012)
2455692.5170	-9594.5	-0.0074	0.0002	(Hubscher et al. 2012)
2455733.3808	-9478.5	-0.0067	0.0008	(Arena et al. 2011)
2455741.4831	-9455.5	-0.0066	0.0009	(Hubscher et al. 2012)
2456415.9034	-7541.0	-0.0044	0.0021	(Nelson 2014)
2457245.8487	-5185.0	-0.0039	0.0008	ASAS-SN (Shappee et al. 2014; Kochanek et al. 2017)
2457246.0255	-5184.5	-0.0032	0.0015	ASAS-SN (Shappee et al. 2014; Kochanek et al. 2017)
2459071.4856	-2.5	0.0012	-0.0002	This paper
2459072.3651	0.0	0.0000	-0.0014	This paper
2459075.3610	8.5	0.0017	0.0003	This paper

Table 7 Target Temperatures

Target	T_{g-i}	T_{g-i}^{der}	T_G	T_{J-K}^{der}	T_m
NSVS 2443858	5631	5766	5375	5922	5840
NSVS 780649	5588	5706	5574	5265	5490
V1098 Her	5932	6027	6208	6060	6080

3.3 V1098 Her

V1098 Her (GSC 03518-00536, NSVS 5320567, ROTSE1 J173937.28 + 501202.0). The ephemeris from the AAVSO VSX is the following

$$HJD(\text{Min } I) = 2455417.2183 + 0.352268564 \times E. \quad (4)$$

Among all data sets, V1098 Her is the star with the greatest number of minima available from literature (Table 6), all well resolved by means of a 2 degree polynomial

ephemeris as follows (Eq. (5))

$$HJD(\text{Min } I) = 2455417.2187(3) + 0.3522688(1) \times E + 5.792^{-11} (\pm 5.236^{-12}) \times E^2. \quad (5)$$

Using the quadratic ephemerides of NSVS 2443858 and V1098 Her as given in Equations (2) and (5), we calculate the rate of period change, dP/dt , utilizing the following formula according to a small quadratic term in the residuals $O - C$, $dP/dE = 2a$, and it reveals for NSVS 2443858 a continuous period increase at the rate of $+2.62 \times 10^{-7} \text{ d yr}^{-1}$ which corresponds to 0.02 s yr^{-1} ; for V1098 Her the continuous period increases at the rate of $+1.20 \times 10^{-7} \text{ d yr}^{-1}$ which corresponds to 0.01 s yr^{-1} .

As one can see from Figures 1 and 2 (left panels), the likely reason for the parabolic shape of the $O - C$ data for NSVS 2443858 and V1098 Her is a transfer of matter between their components.

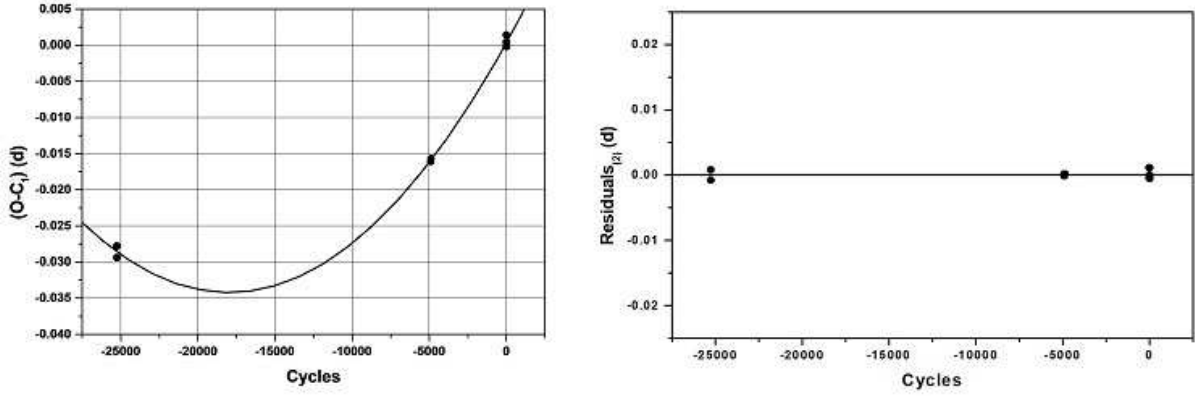


Fig. 1 $O - C$ diagram of NSVS 2443858. (Left panel): The solid line signifies the second-order polynomial fit to Eq. (1). (Right panel): The residuals with respect to Eq. (2) are displayed.

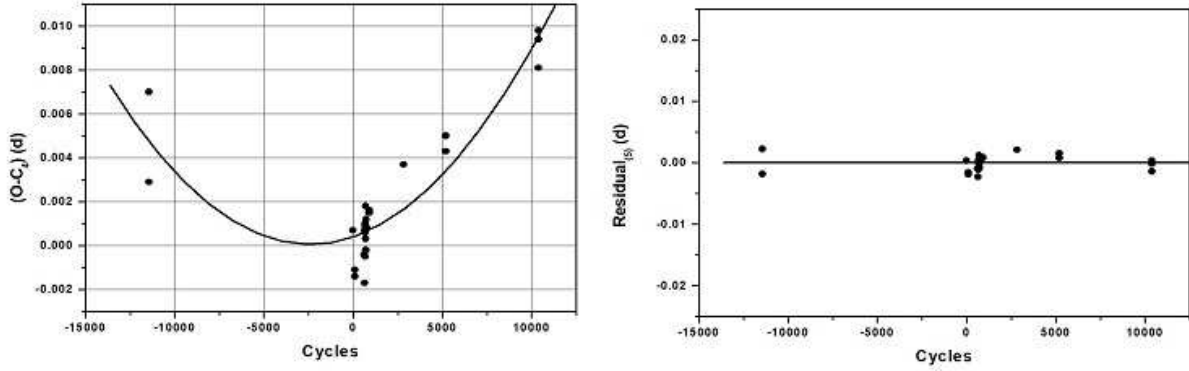


Fig. 2 The same as Fig. 1 but for V1098 Her.

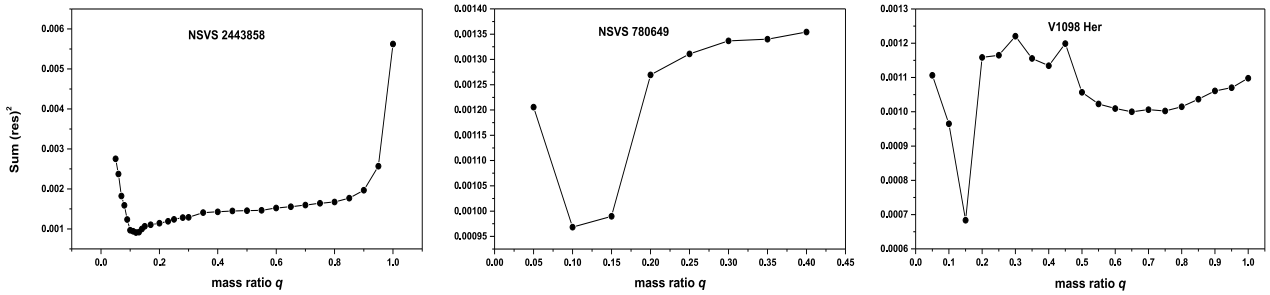


Fig. 3 The relation $\Sigma(res)^2$ versus mass ratio q in Mode 3 for the three systems in the W-D code.

In the case of conservative mass transfer, the rate of mass transfer can be estimated using the formula

$$\frac{dM_2}{dt} = \frac{M_1 M_2}{3P(M_1 - M_2)} \frac{dP}{dt} \quad (6)$$

that is $4.72 \times 10^{-8} M_{\odot} \text{ yr}^{-1}$ for NSVS 2443858 and $1.99 \times 10^{-8} M_{\odot} \text{ yr}^{-1}$ for V1098 Her.

4 ANALYZING AND MODELING THE LIGHT CURVES

The latest version of the Wilson-Devinney (W-D) code (Wilson & Devinney 1971; Wilson 1990; Wilson and van Hamme 2015) was utilized in the analysis of our systems.

Analysis was done for the available g' and i' light curves and the convergence of the minimization procedure

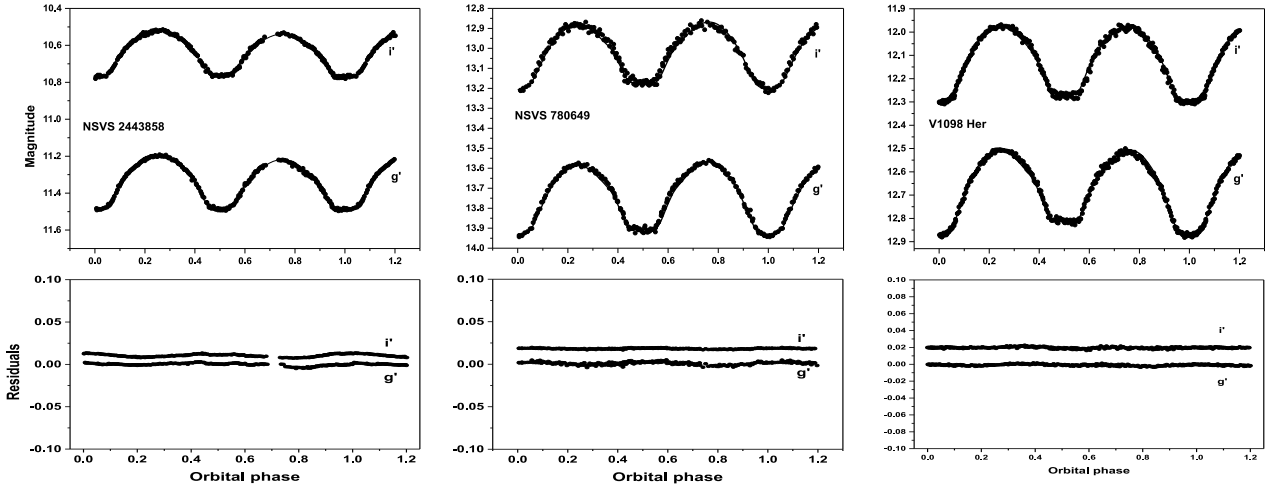


Fig. 4 CCD light curves of the three systems. The points are the original photometric observations and the continuous lines are the theoretical fits with the surface spot contribution. In the lower part of the graph, the residuals are displayed.

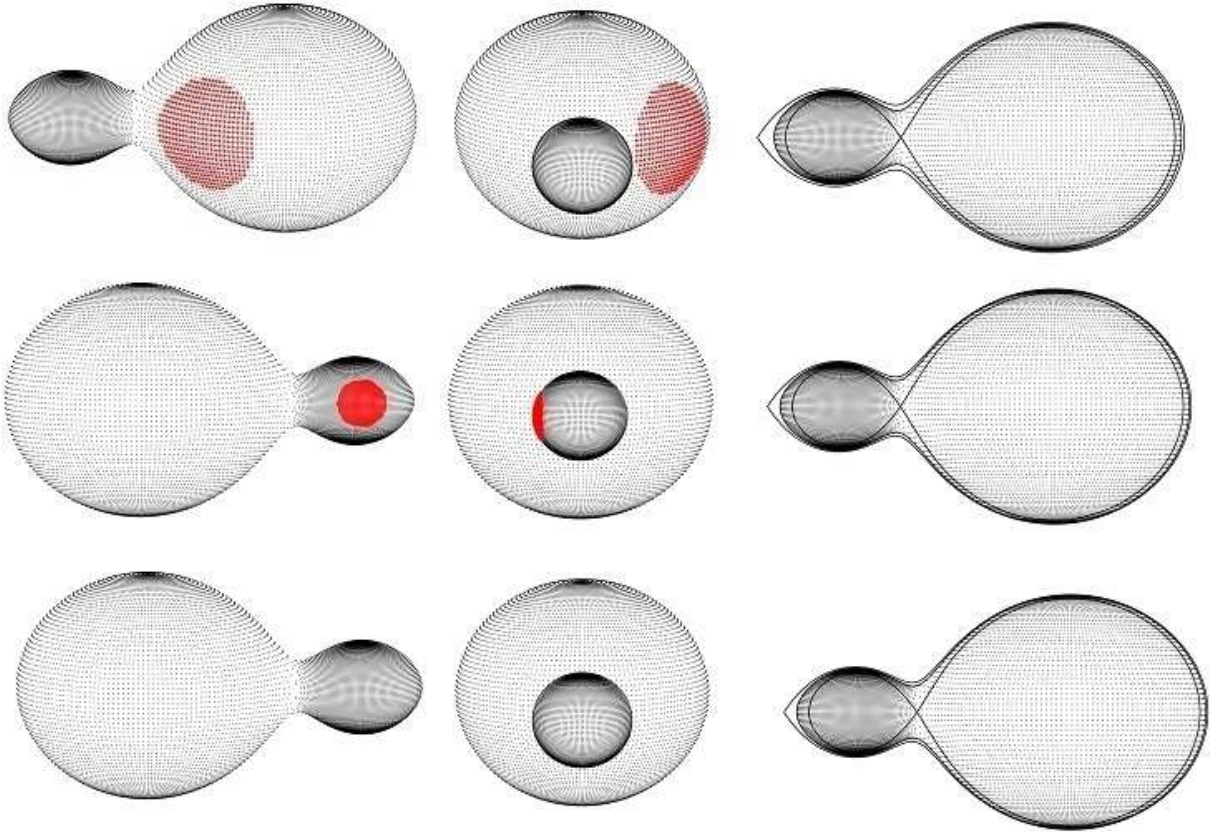


Fig. 5 Graphic images of NSVS 2443858 (*top*), NSVS 780649 (*middle*) and V1098 Her (*bottom*), at quadrature (*left*), at the primary minimum (*center*) and the Roche geometry of the system according to our solution (*right*).

was obtained by means of the multiple subset method (Wilson & Biermann 1976).

Prior to the modeling and fitting procedure, the effective temperature of the eclipsing binary stars should be determined. The de-reddened magnitudes were calculated based on the empirical tables (relations) “temperature –

color index”. The interstellar reddening of our targets was estimated by taking into account the absorptions A_V from Schlafly & Finkbeiner (2011).

The effective temperatures determined in different ways are described in Table 7: T_{g-i} is derived by the measured index ($g' - i'$) at quadrature and the

relation of [Covey et al. \(2007\)](#); T_{g-i}^{der} is the calculated value after dereddening; T_G is the Gaia Data Release 2 (DR2) temperature ([Gaia Collaboration et al. 2018](#)); T_{J-K}^{der} is determined by the 2MASS index ($J - K$) ([Skrutskie et al. 2006](#)) after dereddening and the relation of [Pecaut & Mamajek \(2013\)](#). The last column indicates the assumed target effective temperatures T_m that are equal to the averaged value of T_{g-i}^{der} and T_{J-K}^{der} .

For all three systems the q -search method was performed to find the best initial value of q .

The W-D code was used in Mode 3 (overcontact configuration), correct for typical W UMa-type binary stars.

The gravity darkening and bolometric albedo exponents were set appropriate for convective envelopes ($T_{\text{eff}} < 7500$ K). Limb-darkening coefficients of the components were interpolated from the square root law of the [Claret & Bloemen \(2011\)](#) tables.

During execution of the code, some parameters were treated as adjustable; they are: the inclination of the systems i , the mean temperature of the secondaries T_2 , the surface potentials Ω and the monochromatic luminosity of the primaries L_1 .

The presence of a third light was considered but results showed that its contribution was meaningless for NSVS 780649 and V1098 Her, while for NSVS 2443858 the presence of a visible star close (about 3.5 arcsec) to the system contributes to its total luminosity. For this reason we also left L_3 as a free parameter.

As can be seen in [Figure 3](#), there is a clear indication of the minimum $\Sigma(\text{res})^2$ in the q -search for the three systems.

The following step was to also add the value of the mass ratio corresponding to the minimum of $\Sigma(\text{res})^2$ to the list of adjustable parameters.

A difference in the heights of the maxima in light curves of short-period binaries indicates the presence of the O'Connell effect ([O'Connell 1951](#)) and is attributed to spot activity on the stellar photospheres which can be modeled by hot or cool spots on the components of the systems.

Two of the systems show this characteristic. NSVS 2443858 with the primary maxima being brighter than the secondary while the opposite is true for NSVS 780649 (inverse O'Connell effect).

A new run of the W-D code was used for also adjusting the spot parameters, i.e. co-latitude θ , longitude φ , angular radius γ and temperature factor T_s/T_* .

A cool dark area on the surface of the secondary component of NSVS 2443858 and on the surface of the

primary component of NSVS 780649 allows us to reach a better fit for the light curves.

[Table 8](#) lists the whole final set of accepted parameters from the W-D analysis used to reproduce, as continuous lines, the behavior of the systems among the original data points in [Figure 4](#).

In [Figure 5](#), the graphical representation of the systems and the relative Roche geometries are displayed.

By examining [Tables 8 and 9](#) some information can be obtained:

- NSVS 780649 is W-subtype while the others, NSVS 2443858 and V1098 Her, are A-subtype W UMa systems.

- All three systems have mass ratios close to the established mass ratio limit and belong to the class of deep low mass ratio (DLMR).

- All three systems are binaries with a high orbital inclination.

- While the light curves of NSVS 2443858 exhibit an evident O'Connell effect ([O'Connell 1951](#)), the light curves of NSVS 780649 indicate the inverse O'Connell effect with the secondary maximum higher than the primary one, and the light curves of V1098 Her do not reveal asymmetries.

- A good thermal contact was observed in all the systems but in NSVS 780649 the temperature of the secondary component is ~ 216 K higher with respect to the temperature of the primary one.

Note that the errors of the parameters given in [Table 8](#) are the formal errors from the W-D code. For a discussion see [Barani et al. \(2017\)](#).

5 ESTIMATE OF THE ABSOLUTE ELEMENTS

For two systems, NSVS 780649 and V1098 Her, using the precise distances available in the Gaia database, we manage to estimate the targets' absolute parameters. The procedure that we follow was created especially for the two band g' and i' photometry and is described in [Kjurkchieva et al. \(2019\)](#). The methodology requires the determination of the stars' V magnitudes in quadrature, and it is important particularly for the targets like ours that have deep eclipses.

The available magnitudes in stellar catalogs and those included in large survey databases do not provide information about the epochs of their photometric measurements. The lack of an exact epoch does not allow estimations of the magnitudes in the corresponding phases. To overcome these problems, we estimate our transformed g' magnitudes in quadrature. Then we calculate the V magnitudes utilizing equations (23) of [Fukugita et al. \(1996\)](#) by means of the $(B - V)$ indices corresponding to the target effective temperatures. Taking into account the

Table 8 Values of the Fitted Parameters

Target	$\Omega_{1,2}$	q	i ($^\circ$)	T_1 (K)	T_2 (K)	θ ($^\circ$)	φ ($^\circ$)	γ ($^\circ$)	Ts/T*
NSVS 2443858	1.9775 (20)	0.125 (1)	79.01 (16)	5840 (fxd)	5830 (21)	93.5 (1.1)	52.35 (1.4)	27.7 (3.1)	0.98 (1)
NSVS 780649	1.9032 (6)	0.098 (2)	86.33 (1.7)	5490 (fxd)	5706 (23)	90.0 (fxd)	103.4 (3.3)	30.2 (4)	0.94 (3)
V1098 Her	1.9850 (33)	0.127 (1)	82.62 (22)	6080 (fxd)	5968 (13)	-	-	-	-

Table 9 Calculated Parameters

Target	r_1	r_2	f	T_1^f	T_2^f	l_1	l_2	l_3
NSVS 2443858	0.586 (2)	0.251 (7)	0.705	5840 (fixed)	5830 (21)	0.700 (22)	0.170 (12)	0.152 (4)
NSVS 780649	0.605 (2)	0.226 (2)	0.790	5490 (fixed)	5706 (23)	0.853 (14)	0.124 (10)	0
V1098 Her	0.582 (2)	0.247 (5)	0.644	6080 (fixed)	5968 (13)	0.853 (2)	0.136 (8)	0

Table 10 Absolute Parameters

Target	d (pc)	L_1 (L_\odot)	L_2 (L_\odot)	R_1 (R_\odot)	R_2 (R_\odot)	a (R_\odot)	M_1 (M_\odot)	M_2 (M_\odot)	Sp.type
NSVS 2443858	237 (2)	1.636 (1)	0.298 (2)	1.253 (4)	0.537 (1)	2.144 (4)	1.129 (6)	0.141 (1)	G1 + G1
NSVS 780649	480 (7)	0.995 (44)	0.145 (4)	1.103 (24)	0.390 (1)	1.726 (5)	0.793 (9)	0.078 (1)	G8 + G3
V1098 Her	500 (7)	2.355 (57)	0.377 (15)	1.383 (39)	0.574 (4)	2.324 (17)	1.202 (28)	0.153 (2)	F9 + G0

Spectral types are according to [Pecaut & Mamajek \(2013\)](#).

dust absorptions A_V from [Schlafly & Finkbeiner \(2011\)](#), we estimate the de-reddened V magnitudes.

Relying on the formula for distance modulus, we can calculate the absolute stellar magnitude M_V from the de-reddened V magnitudes. The next formalized steps are to calculate the targets' bolometric absolute magnitudes M_b followed by estimation of their luminosities L_i , stellar radii R_i and masses M_i .

For the third system, NSVS 2443858, the above method does not return a reasonable value of M_1 . For this reason, in estimation of the absolute parameters, we used the three-dimensional (3D) correlation from [Gazeas \(2009\)](#) and the relation between period (in years) and semimajor axis (in a.u.) ([Zhang & Qian 2020](#)).

Table 8 presents the final set of accepted parameters from the W-D analysis, Table 9 lists the calculated parameters and Table 10 features the absolute parameters of our targets.

6 EVOLUTIONAL STATE

To investigate the question what are the evolutionary states of our targets, we examined the MS band of temperature-luminosity ($\log L - \log T$, i.e. Hertzsprung-Russell diagram), mass-luminosity ($\log L - \log M$), mass-radius ($\log R - \log M$) and mass-temperature ($\log T - \log M$) diagrams. We compared the locations of the primary and secondary stellar components as shown on the diagrams of Figure 6. For this purpose we considered

zero age main sequence (ZAMS) and terminal age main sequence (TAMS) isochrones built according to PARSEC models ([Bressan et al. 2012](#)). The results suggest that our systems are binaries consisting of two stars of similar surface brightness but in different evolutionary stages, where the overluminosity of the secondary components (less massive) can be explained by energy transfer from the primary components.

(1) The target components fall almost within the MS band of the $\log T - \log L$ diagram, but the secondaries are slightly overluminous for their temperatures.

(2) The locations of the secondary components above the MS band of the $\log M - \log L$ diagram are indications that their current masses are smaller than the masses of MS stars with similar luminosity. This result is probably due to the processes of mass loss due to rapid evolution. The primaries are around the ZAMS limit. It should be pointed out that the primaries are bigger and more massive than the secondaries, and the targets belong to extreme mass ratio binary (EMRB) systems and two of them, NSVS 2443858 and V1098 Her, have deep contact configurations with fill-out factors bigger than 50%, so they are also DLMR systems.

The conclusion is that the bigger (primary) components are situated around ZAMS than the smaller in size and less massive secondary components of our targets, which are located above the MS band of the $\log M - \log L$ diagram.

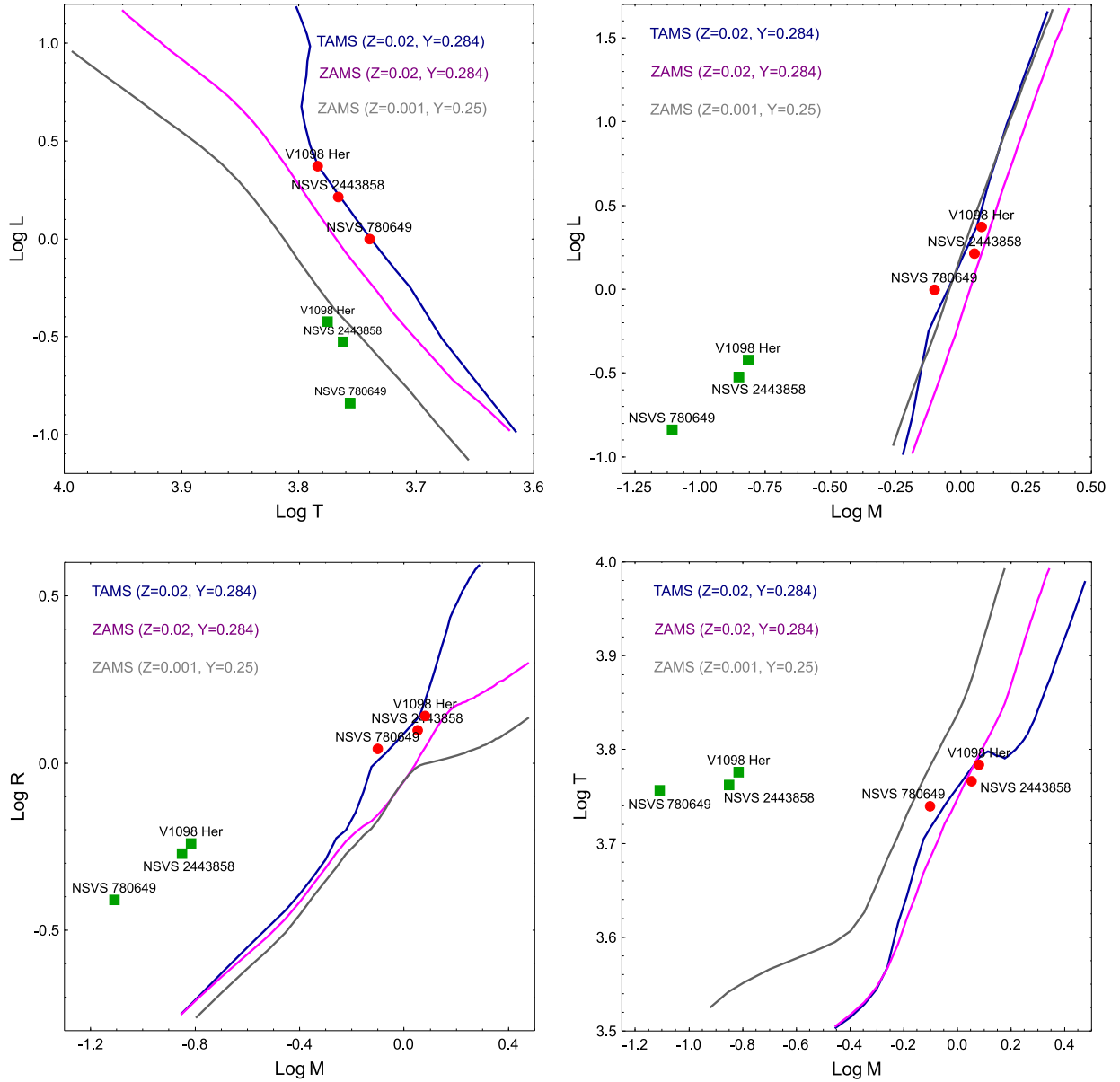


Fig. 6 Properties of our targets plotted against evolutionary tracks of $\log T - \log L$, $\log M - \log L$, $\log M - \log R$ and $\log M - \log T$ (Bressan et al. 2012). The primaries are marked with red circles while the secondaries with green squares.

(3) The secondaries are located above the MS band of the $\log M - \log R$ diagram.

The primary components are within the ZAMS limit. Thus, the conclusion is that the target components that are smaller in size are located above the MS band of the $\log M - \log R$ diagram while the larger primary components do not exceed the ZAMS limit.

(4) The secondaries are located above the MS band of the $\log M - \log T$ diagram, i.e. they are hotter than the MS stars with the same mass. The primaries are within the ZAMS limit. Hence, we may conclude that the components of the targets that are smaller in size are located above the MS band of the $\log M - \log T$ diagram while the

bigger components are around ZAMS. The facts are that the primaries are close to the ZAMS while the secondary components of our targets that are smaller in size are situated above the MS band of the $\log M - \log T$ diagram.

The relations between the calculated absolute parameters of our targets (totally-eclipsing W UMa stars) differ significantly from the parameters of the stars belonging to MS.

This result is a consequence of binary evolution due to energy and mass exchange of the components and their internal transformations. The small ratios of the W UMa stars are indications of an advanced evolutionary stage (Liu et al. 2018).

7 DISCUSSION ON THE SYSTEMS AND CONCLUSION

Here we have presented the analysis of filtered CCD light curves of three short-period contact EMRBs with the mass ratio values (q) ranging from 0.098 to 0.127.

These values are near the theoretical minimum value of mass ratio for W UMa systems. The discussion is still open with the mass ratio values between $q_{\min} \sim 0.09$ (Rasio & Shapiro 1995); $q_{\min} \sim 0.071$ – 0.076 (Li & Zhang 2006); $q_{\min} \sim 0.094$ – 0.109 (Arbutina 2007); $q_{\min} \sim 0.070$ – 0.074 (Arbutina 2012); $q_{\min} \sim 0.044$ (Yang & Qian 2015). We can presume taking into account the conclusions of Gazeas & Stępień (2008) that high- and medium-mass binaries finish evolution in contact as EMRB in which the secondary has already built a noticeable helium core (Paczyński et al. 2007). Such a binary is soon expected to coalesce into a rapidly rotating blue straggler or a single fast rotating star, possibly a giant of FK Com type (Qian et al. 2006). More contact binaries around the mass ratio limit should be observed and analyzed.

The light curves of our targets present total eclipses and their components have nearly equal temperatures. As was shown by Kähler (2004), both stars exchanging energy can, indeed, be in thermal equilibrium. The work of Yakut & Eggleton (2005) assumed that there is a significant amount of heat transfer between the two components, which can be perceived as confirmation that the two components share a common envelope.

An essential transfer of luminosity from one binary component to the other is necessary to produce the close equality of the component temperatures.

The sum $0.871 M_{\odot}$ of the component masses of NSVS 780649 is below the mass limit of 1.0 – $1.2 M_{\odot}$ assumed for the known contact binary stars (Stępień 2006). This means a mass loss and may imply a later evolutionary stage.

All the systems, having a fill-out value greater than 50%, also belong to the class of the DLMR contact systems (Qian et al. 2005). It is believed that DLMR cases are systems approaching the last stage of contact binary evolution and their possible evolution will merge into a single rapidly-rotating star (Qian et al. 2006).

The high orbital inclination of the three systems suggests that they are totally eclipsing binaries and the parameters obtained by the light curve solutions are reliable (Terrell & Wilson 2005).

The target components fall almost within the MS band of the Hertzsprung-Russell diagram ($\log T - \log L$), but the secondaries are slightly overluminous for their temperatures. The secondary components are located above the MS band of the $\log M - \log L$ diagram, i.e.

they have smaller masses than MS stars with the same luminosity. This result is probably due to the process of mass loss due to rapid evolution.

The light curves of V1098 Her do not reveal asymmetries between the maxima. On the other hand, the light curves of NSVS 2443858 display a visible O’Connell effect (O’Connell 1951) with the secondary maximum lower than the primary one and the light curves of NSVS 780649 show an inverse O’Connell effect.

The inhomogeneity of the surface of one or both of the components, associated with cool or hot spots, is believed to be the cause of this difference in level of light at the maxima.

The light curve effect of NSVS 2443858 can be explained by cool spot activity that has the same nature as solar magnetic spots (Mullan 1975).

The inverse O’Connell effect (O’Connell 1951) observed in the light curves of V1098 Her usually indicates hot spot activity due to the probable impact from mass transfer.

For NSVS 2443858 and V1098 Her, the behavior of the $O - C$ diagrams, exhibiting increasing periods, can be explained by mass transfer from the less massive components to the more massive ones.

The spectral types of the components are derived according to table 5 of Pecaut & Mamajek (2013) and are listed in Table 10.

According to the obtained parameters of the systems, 3D graphic representations of the Roche geometries of the three systems are depicted in Figure 5 using Binary Maker ver. 3.0 (Bradstreet & Steelman 2002).

Acknowledgements The research was supported partly by project DN08/20 of Scientific Foundation of the Bulgarian Ministry of Education and Science, and project RD 0-92/2019 of Shumen University. The research was made with the support of the private IRIDA OBSERVATORY². This work has made use of data from the European Space Agency (ESA) mission Gaia, processed by the Gaia Data Processing and Analysis Consortium (DPAC). Funding for the DPAC has been provided by national institutions, in particular the institutions participating in the Gaia Multilateral Agreement. This research also has made use of the SIMBAD database, operated at CDS, Strasbourg, France, NASA Astrophysics Data System Abstract Service. We acknowledge our anonymous referee for comments that helped to improve this work.

References

Akerlof, C., Amrose, S., Balsano, R., et al. 2000, AJ, 119, 1901

² <http://www.irida-observatory.org>

- Arbutina, B. 2007, *MNRAS*, 377, 1635
- Arbutina, B. 2012, *Publications de l'Observatoire Astronomique de Beograd*, 91, 391
- Arena, C., Aceti, P., Banfi, M., et al. 2011, *Information Bulletin on Variable Stars*, 5997, 1
- Bailer-Jones, C. A. L., Rybizki, J., Fouesneau, M., Mantelet, G., & Andrae, R. 2018, *AJ*, 156, 58
- Barani, C., Martignoni, M., & Acerbi, F. 2017, *New Astron.*, 50, 73
- Berdyugina, S. V. 2005, *Living Reviews in Solar Physics*, 2, 8
- Berry, R., Burnell, J., 2006. *The Handbook of Astronomical Image Processing with AIP4WIN2 Software*, Willmann-Bell, Inc., WEB
- Binnendijk, L. 1970, *Vistas in Astronomy*, 12, 217
- Bradstreet, D. H., & Steelman, D. P. 2002, in *American Astronomical Society Meeting Abstracts*, 201, 75.02
- Brat, L., Trnka, J., Smelcer, L., et al. 2011, *Open European Journal on Variable Stars*, 137, 1
- Bressan, A., Marigo, P., Girardi, L., et al. 2012, *MNRAS*, 427, 127
- Claret, A., & Bloemen, S. 2011, *A&A*, 529, A75
- Covey, K. R., Ivezić, Ž., Schlegel, D., et al. 2007, *AJ*, 134, 2398
- de Ponthire, P., 2010. *LESVEPHOTOMETRY*, Automatic Photometry Software (<http://www.dppobservatory.net>).
- Eggleton, P. P., & Kiseleva-Eggleton, L. 2001, *ApJ*, 562, 1012
- Fukugita, M., Ichikawa, T., Gunn, J. E., et al. 1996, *AJ*, 111, 1748
- Gaia Collaboration, Brown, A. G. A., Vallenari, A., et al. 2018, *A&A*, 616, A1
- Gazeas, K. D. 2009, *Communications in Asteroseismology*, 159, 129
- Gazeas, K., & Stępień, K. 2008, *MNRAS*, 390, 1577
- Gettel, S. J., Geske, M. T., & McKay, T. A. 2006, *AJ*, 131, 621
- Henden, A. A., Levine, S., Terrell, D., & Welch, D. L. 2015, in *American Astronomical Society Meeting Abstracts*, 225, 336.16
- Hoňková, K., Juryšek, J., Lehký, M., et al. 2013, *Open European Journal on Variable Stars*, 160, 1
- Hubscher, J., Lehmann, P. B., & Walter, F. 2012, *Information Bulletin on Variable Stars*, 6010, 1
- Jayasinghe, T., Stanek, K. Z., Kochanek, C. S., et al. 2020, *MNRAS*, 491, 13
- Kähler, H. 2004, *A&A*, 414, 317
- Kjurkchieva, D. P., Popov, V. A., Eneva, Y., & Petrov, N. I. 2019, *RAA (Research in Astronomy and Astrophysics)*, 19, 014
- Kjurkchieva, D. P., Popov, V. A., & Petrov, N. I. 2018, *RAA (Research in Astronomy and Astrophysics)*, 18, 129
- Kochanek, C. S., Shappee, B. J., Stanek, K. Z., et al. 2017, *PASP*, 129, 104502
- Li, L., & Zhang, F. 2006, *MNRAS*, 369, 2001
- Liu, L., Qian, S. B., & Xiong, X. 2018, *MNRAS*, 474, 5199
- Lucy, L. B. 1968a, *ApJ*, 153, 877
- Lucy, L. B. 1968b, *ApJ*, 151, 1123
- Mullan, D. J. 1975, *ApJ*, 198, 563
- Nelson, R. H. 2014, *Information Bulletin on Variable Stars*, 6092, 1
- O'Connell, D. J. K. 1951, *Publications of the Riverview College Observatory*, 2, 85
- Paczyński, B., Sienkiewicz, R., & Szczygieł, D. M. 2007, *MNRAS*, 378, 961
- Pecaut, M. J., & Mamajek, E. E. 2013, *ApJS*, 208, 9
- Qian, S. B., Yang, Y. G., Soonthornthum, B., et al. 2005, *AJ*, 130, 224
- Qian, S., Yang, Y., Zhu, L., He, J., & Yuan, J. 2006, *Ap&SS*, 304, 25
- Rasio, F. A., & Shapiro, S. L. 1995, *ApJ*, 438, 887
- Rucinski, S. M. 2001, *AJ*, 122, 1007
- Schlafly, E. F., & Finkbeiner, D. P. 2011, *ApJ*, 737, 103
- Shappee, B. J., Prieto, J. L., Grupe, D., et al. 2014, *ApJ*, 788, 48
- Skrutskie, M. F., Cutri, R. M., Stiening, R., et al. 2006, *AJ*, 131, 1163
- Stepien, K. 2006, *Acta Astronomica*, 56, 347
- Terrell, D., & Wilson, R. E. 2005, *Ap&SS*, 296, 221
- Webbink, R. F. 1976, *ApJ*, 209, 829
- Wilson, R. E. 1990, *ApJ*, 356, 613
- Wilson, R. E., & Biermann, P. 1976, *A&A*, 48, 349
- Wilson, R. E., & Devinney, E. J. 1971, *ApJ*, 166, 605
- Wilson, R. E., & van Hamme, W. 2015, *Computing Binary Stars Observables*, <ftp.astro.ufl.edu/directorypub/wilson/lcdc2015>
- Woźniak, P. R., Vestrand, W. T., Akerlof, C. W., et al. 2004, *AJ*, 127, 2436
- Yakut, K., & Eggleton, P. P. 2005, *ApJ*, 629, 1055
- Yang, Y.-G., & Qian, S.-B. 2015, *AJ*, 150, 69
- Zhang, X.-D., & Qian, S.-B. 2020, *MNRAS*, 497, 3493